

Adaptive, Cricket-Inspired Artificial Hair Sensor Arrays

R. K. Jaganatharaja, N. Izadi, J. Floris, T. S. J. Lammerink, R. J. Wiegerink and G. J. M. Krijnen

Abstract—In this work, we present a model for our biomimetic, artificial hair sensors, to analyze the sensitivity dependence on their structural and geometrical parameters. Based on this model, feasible design improvements to achieve an increased sensitivity are discussed and a figure of merit to evaluate sensor performance is defined. Also, we discuss the results of a novel approach to implement adaptive sensor arrays through DC-biasing based on the electrostatic spring-softening effect. Experimental results show a clear theoretical accordance and tunability of system's resonance frequency, providing opportunities for frequency focusing and selective sensitivity.

Index Terms—adaptivity, artificial hair sensors, biomimetics, spring-softening

I. INTRODUCTION

Crickets have, quite often, been a subject of common interest to biologists and engineers. They have evolved with a pair of special flow-sensitive appendices called cerci with numerous mechano-receptive filiform hairs of different lengths, distributed on the surface.

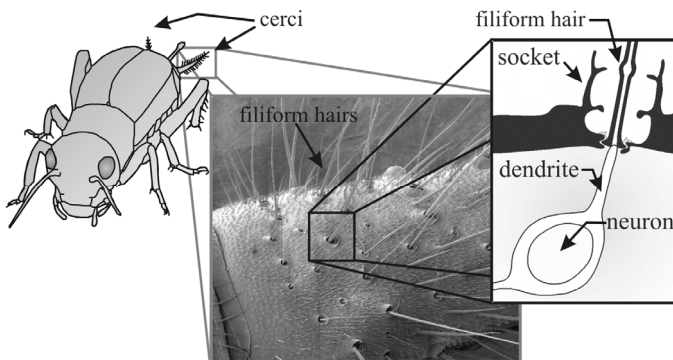


Fig. 1. Mechano-receptive hairs found on cerci of crickets. [SEM image courtesy by Jerome Casas, IRBI, Université de Tours.]

These filiform hairs are extremely sensitive to acoustic signals, down to thermal noise levels [1], enabling them to identify and escape from approaching predators. Each filiform hair has a mechano-sensitive neuron at its base which fires a neuro-signal whenever there is a flow-induced deflection on the hair, see Fig. 1.

Inspired by crickets and making use of technical advancements in MEMS techniques, SU-8 based artificial hair sensor arrays were successfully implemented recently [2]. Ways to improve the sensitivity of these artificial hair sensor arrays have been demonstrated; increasing the hair length and arranging the sensors on an artificial cercus-like platform that can be assembled to facilitate 3D-flow sensing, see Fig. 2.

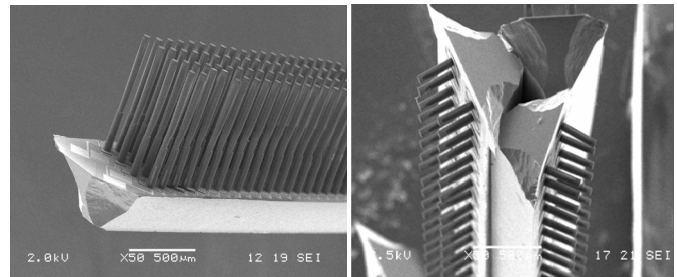


Fig. 2. SEM images of the realized biomimetic hair sensor arrays, arranged on the artificial cerci-like substrate.

In this work, we present a model for our artificial hair sensor to further study and optimize the effects of structural and geometrical parameters on the sensitivity and a figure of merit for our sensors is defined based on this model. Parallel to this, we present a new approach to develop adaptive hair sensors which are tunable with respect to the best frequency and sensitivity [3].

II. PRINCIPLE OF OPERATION

The artificial hair sensor is based on a differential capacitive sensing technique. Drag-torque due to the air flow, picked-up by the SU-8 hair, results in a membrane tilt. This flow-induced tilting of silicon (rich) nitride (SiRN) membrane with electrodes on top, causes a change in the sensor capacitance, with respect to the bottom electrode (bulk silicon), see Fig. 3. The capacitance change is read-out using charge amplifiers and synchronous detection [2].

Manuscript received October 1, 2007. This work was done as a part of Bio-EARS (funded by STW/NWO) and CILIA projects. The Customized Intelligent Life-Inspired Arrays (CILIA) project is funded by the Future and Emergent Technologies arm of the IST Program.

All the authors are with the Transducer Science and Technology group, MESA+ and IMPACT Research Institutes, University of Twente, Postbus 217, 7500 AE Enschede The Netherlands (phone: 053-489-4438; fax: 053-489-3343; email: r.kottumakulal@ewi.utwente.nl).

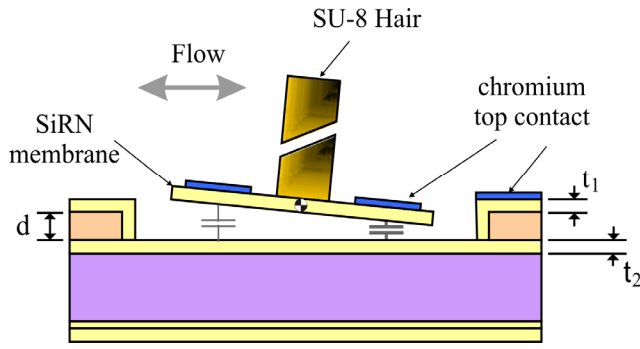


Fig. 3. Schematic of the hair sensor.

III. SENSOR MODEL

A. Sensitivity

The structural functionality of cricket hairs has been described in terms of mechanical and hydrodynamic models in literature [4,5]. Whereas biologists have used the models to arrive at estimates of the mechanical properties of the hairs (hair moment of inertia J , torsional spring constant S and torsional resistance R), we have implemented the model to optimize our sensor design with respect to actual sensor properties.

The normalised sensitivity dC/dV_0 (C the capacitance and V_0 the far-field flow velocity amplitude) can be approximated by the product of: (i) the hydrodynamic torque pick-up by the hairs, (ii) the second-order mechanical system response, and (iii) the capacitance change per unit of rotation of the membrane (F/rad) [3]. The approximation lies in assuming that the velocity of the tip of the hairs is much smaller than the flow velocity itself.

The hairs are deflected by viscous drag on the hair shaft due to particle velocity. For harmonic flow velocities parallel to a flat surface given by a far-field of the form

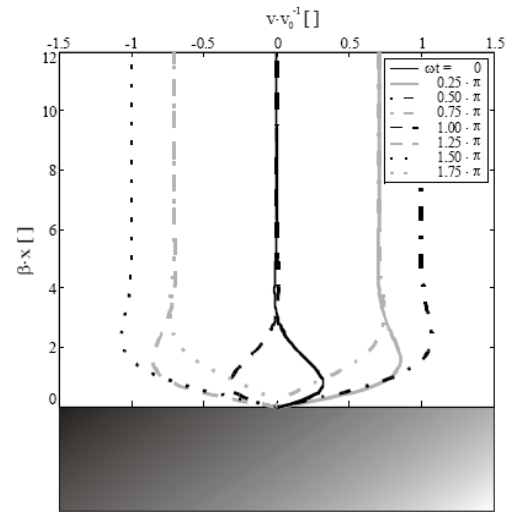
$$v_{y,\infty}(t) = V_0 \cdot \sin(\omega t) \quad (1)$$

The frequency dependent velocity profile above the surface is given by [6,7]:

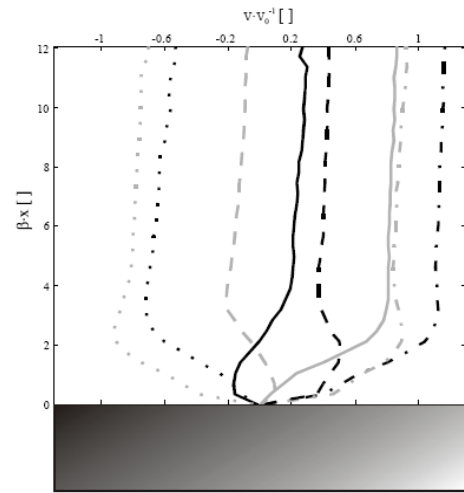
$$v_y(x,t) = V_0 \cdot \sin(\omega t) - V_0 \cdot e^{-\beta x} \cdot \sin(\omega t - \beta x) \quad (2)$$

$$\beta = \sqrt{\frac{\omega}{2 \cdot \nu}}$$

with ν the kinematic viscosity, x the distance from the surface and ω the angular frequency of the harmonically oscillating flow. Due to viscosity and no-slip at the interface between fluid and fixed surface there is a transition zone between zero velocity and the far-field velocity, the so-called boundary layer. The boundary layer thickness (δ_b) depends on $2/\beta$, being larger at lower frequencies. Fig. 4 shows calculated and measured normalized flow-profiles above flat surfaces for various time-instants of one period of oscillation. Agreement between both is excellent permitting to use Eqn. (2) in further modeling approaches.



(a)



(b)

Fig. 4. Oscillating boundary layer on a flat surface, (a) calculated, (b) measured using a Particle Image Velocimetry setup, normalized with: $v_{\text{air}} = 1.79 \cdot 10^{-5} \text{ N} \cdot \text{s} \cdot \text{m}^{-2}$, $v_0 = 3 \text{ cm} \cdot \text{s}^{-1}$ and $f = 60 \text{ Hz}$. [Measurements by Thomas Steinmann *et al.*, IRBI, Université de Tours].

In the small Reynolds number regime the drag-forces can be described by the Stokes expressions. These state that the drag-force by a fluid-flow given by Eqn. (1) on a cylinder of unit length is given by [4,5]:

$$F_d(t) = \left\{ 4\pi\mu \cdot \frac{-g}{g^2 + (\pi/4)^2} \right\} V_0 \cdot \sin(\omega t) \quad (3)$$

$$+ \omega \left\{ \pi\rho_a a^2 + \frac{4\pi\mu}{\omega} \cdot \frac{\pi/4}{g^2 + (\pi/4)^2} \right\} V_0 \cdot \cos(\omega t)$$

with μ the dynamic viscosity, a the radius of the cylinder and ρ_a the mass-density of air. The variable g is given by:

$$g = \ln(a\beta/\sqrt{2}) + \gamma \quad (4)$$

where γ is Euler's constant (0.5772..).

The velocity in Eqn. (3) is actually the velocity difference between the flow and the hair. However, the stiffness of our hairs is on the order of 10^{-8} Nm/rad and hair movement is relatively small in our structures so that the velocity difference can be approximated by the flow velocity itself (Eqn. (1)). The total torque on the filiform hairs can be calculated by integrating the drag moment along the hair:

$$T_d = \int_0^{L_h} F_d(x) \cdot x \cdot dx \quad (5)$$

Using Eqns. (2), (3) and (5), the total drag-torque on the hairs can be determined. The integration of Eqn. (5) is readily done numerically.

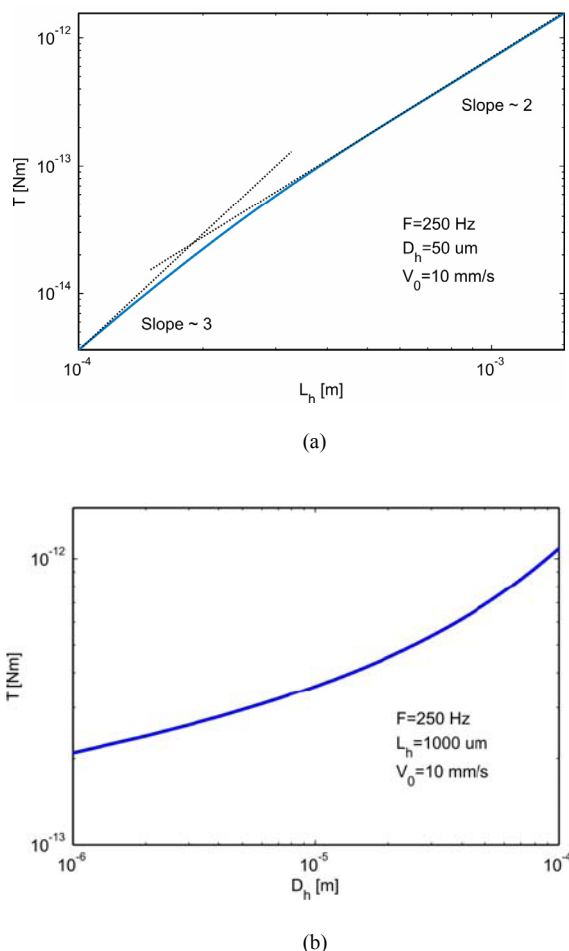


Fig. 5. (a) Drag-torque on hairs, vs. hair length (model) and (b) Drag-torque on hairs, vs. hair diameter (model)

Using the model we investigated the dependence of the sensitivity as a function of hair-length, see Fig. 5(a). The drag-torque increases approximately proportional to the hair length cubed (L_h^3), when L_h is smaller than the boundary layer thickness (δ_b) and with approximately $(L_h)^2$ when $L_h > \delta_b$. On the other hand, changing the diameter of the hairs is by far not as influential (Fig. 5(b))

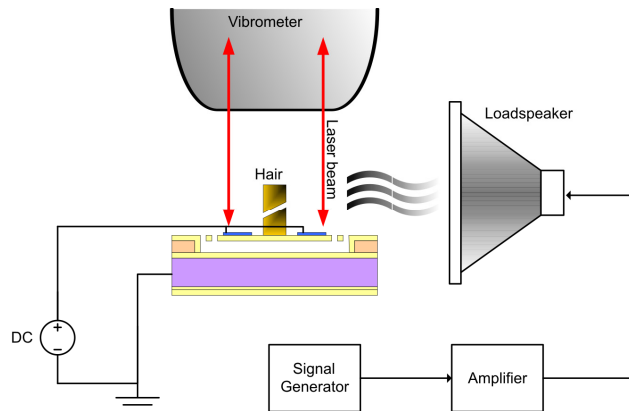


Fig. 6. Schematic of the experimental set-up using loudspeaker as a very-near field sound source and laser-vibrometer for detecting the membrane deflection.

Experimental results were obtained using a laser-vibrometer and acoustic excitation by a small loudspeaker in the very-near field [8], see Fig. 6. For comparison the model-results are shown in Fig. 7. The only chosen parameter in these calculations is the quality factor; other values (J , S , T_{drag} etc) were directly obtained from the hydro-dynamics and structural properties. Model and measurements are in good agreement both with respect to the frequency dependence and to the absolute sensitivity values.

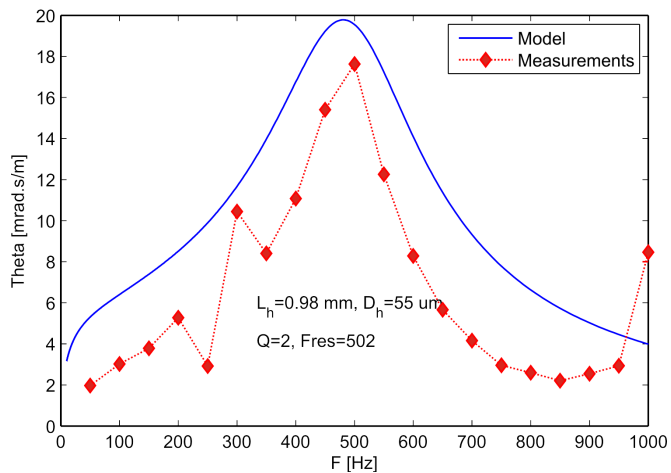


Fig. 7. Measured (optically) and modeled normalized sensitivity of realized hair sensors Vs. frequency.

B. Figure of Merit (FoM)

In order to optimize the hair-sensors and to allow a comparison between artificial and natural hair-sensors we make the following observations. a) When the torsional spring stiffness is low, the drag-induced rotations are large providing high sensitivity. Hence a low rotational stiffness seems desirable. b) The resonance frequency of the hairs depends on the torsional stiffness S , the lower S the lower the resonance frequency ω_0 at given moment of inertia J . It is not unreasonable to take the resonance frequency ω_0 as a measure for the bandwidth in which the sensors can be used since

above this frequency the response decreases with 12dB/octave. c) Longer hairs do experience larger drag-torque than smaller hairs (Fig. 5a) and seem to be desirable for high sensitivity. d) At the same time hair-length L_h occurs cubed³ in the inertial moment J having large impact on ω_0 . e) The diameter of the hairs has a quadratic influence on the inertial moment, but only a very slight effect on drag-torque (Fig. 5(b)). Although depending on frequency, in the frequency range of interest the relation between the drag-torque and the diameters can be approximated by $\alpha (D_h)^{1/3}$.

Sensor-optimisation has (at least) two dimensions: usable bandwidth and (low-frequency) sensitivity. If one of both is (too) low the usability of the sensor is strongly hampered. We have also argued that both sensitivity and bandwidth depend strongly on S , L_h and D_h . Therefore we define a figure of merit (FoM) as the product of usable bandwidth (i.e. proportional to ω_0) and low frequency sensitivity (i.e. the drag-torque to which a hair is exposed divided by the rotational stiffness). Using the above simplifications we arrive at:

$$FoM \equiv \omega_0 \cdot \frac{T_d}{S} = \sqrt{\frac{S}{J}} \cdot \frac{T_d}{S} \quad (6)$$

$$\propto \sqrt{\frac{S}{\rho L_h^3 D_h^2}} \cdot \frac{L_h^2 D_h^{1/3}}{S} = \sqrt{\frac{L_h}{\rho S D_h^{4/3}}}$$

This FoM shows that sensitive sensors with a large usable bandwidth should have long, thin hairs made of low density material, and small torsional stiffness, exactly what is seen in nature. In comparing the FoM of the artificial hair-sensors to the FoM of the crickets' hairsensors, we find that cricket hairs perform about a 100 times better mechanically (for 1 mm long hairs). Crickets out-perform artificial sensors because of their low torsional stiffness ($2 \cdot 10^{-11}$ vs. $7 \cdot 10^{-9}$ Nm/rad) and small average hair-diameter (4.5 vs. 50 μm).

IV. ADAPTIVITY

A. Electrostatic Spring Softening

Based on transduction theory, applying a bias voltage on the capacitors results in a change in the effective spring stiffness (see Fig. 8), given as:

$$S_{eff} = S_0 - \frac{U_{bias}^2}{2} \frac{\partial^2 C}{\partial \alpha^2} = S_0 - U_{bias}^2 \kappa \quad (7)$$

where S_{eff} is the effective spring constant, α is the sensor plate angular rotation, S_0 is the physical rotational spring stiffness of the torsional beams, U_{bias} is the applied bias voltage, C is the capacitance of the device and κ is the second derivative of the capacitance with respect to the angle of rotation divided by two.

Since U_{bias}^2 is always positive, an applied bias voltage will give a reduction in the spring stiffness. Therefore DC-biasing results in increasing the tilt angle, at given drag-torque acting on the hairs (and for frequencies below the best frequency), given by:

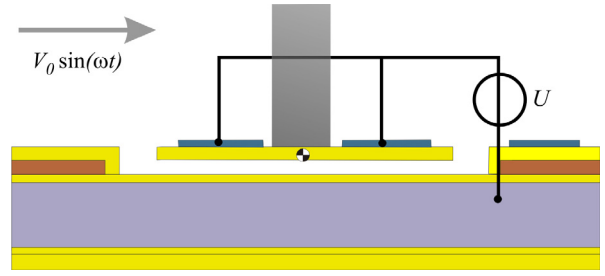


Fig. 8. Electrostatic spring softening effect by applying DC-bias.

$$\alpha = \frac{T(\omega, V_0)}{S_{eff}} = \frac{\alpha_0}{1 - \frac{\kappa}{S_0} U_{bias}^2} \kappa \quad (8)$$

where T is the total drag torque acting on the hair (depending on frequency and far-field velocity amplitude) and α_0 is the angle of rotation for given T without applied DC-bias. By the relation between resonance frequency and spring stiffness, the change in the resonance frequency, ω_0 , by DC-biasing is given as:

$$\omega_0(U_{bias}) = \sqrt{\frac{S(U_{bias})}{I}} = \omega_0(0) \sqrt{1 - \frac{\kappa}{S_0} U_{bias}^2} \quad (9)$$

Here κ/S_0 is a constant depending on the geometry of the structure. From Eqn. (8) and (9) it follows that the hair-sensors can be adaptively changed to accommodate optimal signal reception. Fig. 9 shows various curves for a range of bias voltages between 1.4 V (red curve) and 7.2 V (green curve). Since the mechanical model does not include any physical damping, e.g. such as squeezed film effects, the damping coefficient R has been set to produce a quality factor $Q=2$ at zero bias-voltage and kept constant for the other curves. This results in a decrease of quality factor with increasing bias-voltage (decreasing resonance frequency).

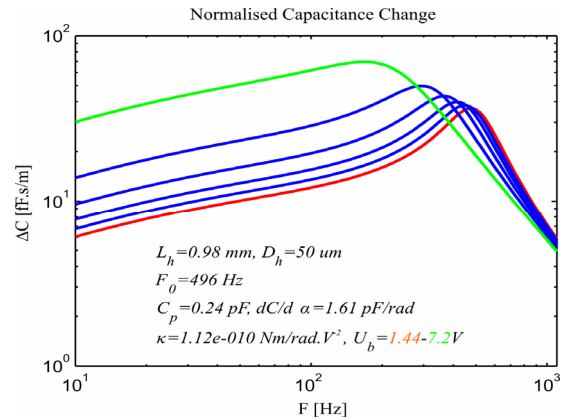


Fig. 9. Model predictions showing the adaptive behavior of sensitivity and resonance frequency for a range of applied bias voltages ($U_{bias} = 1.44-7.2$ V).

In order to estimate the sensitivity to DC-biasing we calculated the coefficient κ . In general this coefficient cannot

easily be calculated analytically for any non-zero α . However, in the case of the hair sensors studied here, with small angles of rotation encountered in practice, κ is calculated as in Eqn. (10) where g is the effective dielectric spacing between the capacitor electrodes and A the surface area of the electrodes.

$$\kappa = \frac{1}{2} \frac{\partial^2}{\partial \alpha^2} \left(\int_A \frac{\epsilon_0 dA}{g(x, y, \alpha)} \right) \Big|_{\alpha=0} \quad (10)$$

$$\approx \lim_{\alpha \rightarrow 0} \frac{1}{2} \int_A \frac{\partial^2}{\partial \alpha^2} \left(\frac{\epsilon_0}{g(x, y, \alpha)} \right) dA$$

Using Eqn. (10) we find for a stress-induced curved circular membrane, with radius R and maximum deflection a at the rim:

$$\kappa = \frac{\pi \epsilon_0}{8a} R^4 \left\{ \frac{1}{t_{eff}^2} - \frac{1}{(t_{eff} + a)^2} \right\} \quad (11)$$

where $t_{eff} = d + (t_{SiRN})/\epsilon_r$, d is the airgap and t_{SiRN} is the total SiRN thickness in the capacitors.

B. Experiments and Results

In order to verify the model predictions on DC-biasing, two types of experiments were conducted:

(1) With the electrical actuation DC-bias voltages applied, resonance frequencies were determined. Fig. 10 shows the measured resonance frequencies for the sensor at different applied DC-bias voltages and the solid line is the model, Eqn. (9), fitted to the measurement data resulting in a value for κ/S_0 of 0.016 V^{-2} .

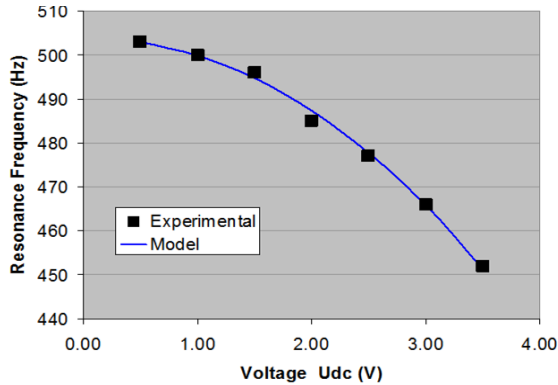


Fig. 10. Resonance frequency Vs. applied DC-bias. Solid line is the least squares fit adjusting the $\omega_0(0)$ and κ/S_0 .

(2) Using acoustic actuation, (a loudspeaker was used to apply the airflow and the sensors were placed in the very near field of a loudspeaker), the membrane rotation normalized to the air flow, at various DC-bias voltages was characterized using a laser vibrometer. Fig. 11 gives the membrane's amplitude of rotation normalized to the applied air flow from the loudspeaker versus the bias voltage at various actuation frequencies. Fitting the measurement data to the model, Eqn. (8), we find a value for κ/S_0 of 0.0171 V^{-2} .

Using the model, the calculated value of κ/S_0 based on the

geometrical and material parameters of the sensors (i.e. without any fit), was 0.0156 V^{-2} , which proves that the model's predictions are relatively close to the experimental values.

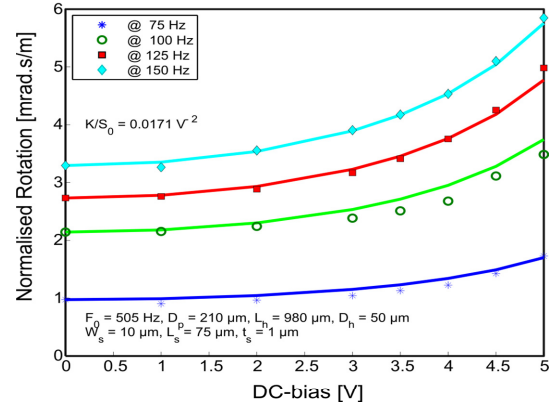


Fig. 11. Normalized membrane rotation by a sinusoidal flow Vs. DC-bias. Parameters are indicated in the figure.

V. CONCLUSION

A model-based optimization scheme and a figure of merit to evaluate sensor performance have been presented. Experimental results correspond well to model predictions. Adaptivity of the sensor based on electrostatic spring softening by DC-biasing has been described and experimentally shown, with good theoretical agreement.

ACKNOWLEDGEMENT

The authors want to thank: Meint de Boer, Erwin Berenschot, and Dominique Altpeter, for their advices on processing of the devices and also our colleagues in the EU project CILIA for their fruitful discussions and inputs to this work.

REFERENCES

- [1] T. Shimozawa, J. Murakami, T. Kumagai, "Cricket wind receptors: thermal noise for the highest sensitivity known", Chapter 10 in *Sensors and Sensing in Biology and Engineering*, ed. Barth, Hamphry and coombs, Springer, Vienna, 2003, ISBN 3-211-83771-X.
- [2] M. Dijkstra et al., "Artificial sensory hairs based on the flow sensitive receptor hairs of crickets", *J. Micromech. and Microeng.*, 15 (2005), 132-138.
- [3] G. J. M. Krijnen, J. Floris, M. A. Dijkstra, T. S. J. Lammerink, and R. J. Wiegink, "Biomimetic micromechanical adaptive flow-sensor arrays", *Proceedings of SPIE Europe Microtechnologies for the New Millennium 2007*, 2-4 May 2007, Maspalomas, Gran Canaria, Spain.
- [4] T. Shimozawa et al., "Structural scaling and functional design of the cercal wind-receptor hairs of cricket", *J. Comp. Physiol. A*, 183 (1998), 171-186.
- [5] J. Humphrey et al., "Dynamics of arthropod filiform hairs. II. Mechanical properties of the hair and air motions", *Philosophical Transactions: Biological Sciences*, Vol. 340, Nr. 1294, pp. 423-444, 1993.
- [6] Cummins, B., Gedeon, T., Klapper, I., Cortez, R., "Interaction between arthropod filiform hairs in a fluid environment", *Journal of Theoretical Biology* Vol. 247, 2007, pp. 266-280.
- [7] Lindken R., Westerweel J., Wieneke B., "Stereoscopic micro particle image velocimetry", *Experiments in Fluids*, Vol. 41, 2006, pp.161-171.
- [8] H-E. de Bree et al., 11th International Congress on Sound and Vibration (ICSV11), St. Petersburg 2004.